

Phase Analysis of Thin Film Oxide Systems by AES and EELS

V.G. Beshenkov, V.A. Marchenko, V.T. Volkov and A.G. Znamenskii

Institute of Microelectronics Technology and High Purity Materials, Russian Academy of Sciences, Chernogolovka, Moscow Region, 142432, Russia

Abstract

Auger electron spectroscopy (AES) and reflection electron energy loss spectroscopy (EELS in a reflection mode) are compared as the methods for phase composition investigation of thin film oxide systems by ion profiling. As an example, the $Al/Al_2O_3/Si$ and $YBa_2Cu_3O_{7-x}/CeO_2/Al_2O_3$ systems are considered. The adaptation of applied statistics methods for the AES and EELS data treatment is discussed.

1. Introduction

Both Auger and electron energy loss spectra display phase composition of materials under study and can be obtained on standard electron spectrometers. Lineshape and energy position sensitivity of Auger line to chemical element bonding as well as electron energy loss structure near elastic peak can be used as "finger prints" of uniphase materials. Due to chemical reactions at the interfaces in thin film systems or surface interaction with atmosphere, the mixtures of different phases occur in the field of analysis and the spectra obtained are overlapped markedly. At the same time, the phase composition information and the data treatment principles are somewhat different in AES and EELS.

The present work is devoted to studying sharp interfaces (up to 5 nm), when the mixing of spectra occurs through the ion beam etching ununiformity and the existence of finite information length for escaping electrons.

2. The method of phase analysis

Imagine a certain Auger spectrum or electron energy loss spectrum in a multidimensional linear vector space. Take the number of coordinate axes equal to the number of accumulated intensities \mathbf{m} in the spectrum and specify coordinates by corresponding intensities. The point obtained is an image of isolated spectrum and represents the object of classification (ordination), when the set of \mathbf{n} spectra is mapped. The sequence of points is consistent with the depth profile and reflects the alteration of phase composition in depth. Due to a partial duplication of the information contained in spectra the geometric configuration of image points can be displayed in a space of low dimensionality. In order to transit into such a space with the lowest distortion of the angles and distances

between the points, the methods of reduction of space dimensionality as principal component analysis or factor analysis can be used [1-3]. In particular, the analyzed data can be projected into the spaces defined by one, two, three, etc. principal components. There exist some tests of applied statistics to define the dimensionality of such a space for which the loss of information by data projection occurs at the cost of random experimental error [2-4]. The most convenient test, to our mind, is the graphical method based on an equivalence of secondary ("noise") eigenvectors in an eigendecomposition of covariance matrix [4]. We decompose $\mathbf{n} \times \mathbf{n}$ covariance matrix $\mathbf{S} = \mathbf{X}^T \mathbf{X}$ (\mathbf{X} - $\mathbf{m} \times \mathbf{n}$ data matrix, $\mathbf{m} > \mathbf{n}$) and use \mathbf{n} column elements \mathbf{h}_{ij} $i=1, \dots, \mathbf{n}$ $j=1, 2$ of the two first eigenvectors as spectra coordinates in the two-dimensional case. The elements \mathbf{h}_{ij} $i=1, \dots, \mathbf{n}$ $j=1, 3$ are additionally used to construct the orthogonal plane in the three-dimensional case. It is quite natural to connect the dimensionality of the space with the phase number in the object under study.

The inherent AES ability to sense Auger lines of different chemical elements enables one to find "uniphase" regions in depth distribution by principal component analysis and to use them for phase concentration calculations, including mixing with the phases unanalyzable on the Auger line under study. One needs to select in the projection map such types of point configurations as point clusters or points on a straight line which contains the origin of coordinates. The objects of classification (spectra in the set) corresponding to that points may be considered as phase references, because the loading coefficients on the phase are unity or can be scaled to unity. Other phases, at the same time, have zero loadings. The loading coefficients deduced by oblique rotation of principal axes for the points composing the interface can be defined as phase concentrations (fractions) at the interface, if the axis scaling is implemented in appropriate manner (new axes are directed to phase references).

In the case of the absence of uniphase regions in depth profile defined by Auger line projecting, there is a need to use the references of chemical compounds. When all the phases are identified in accordance with the number of the phases deduced earlier, the phase concentrations can be obtained by the multiple linear regression method or target transformation procedure [3-4]. The statistical method of phase identification using the references based on the hypothesis test is presented in [5].

One can obtain the statistically unsatisfactory agreement of the oxide references with the oxide system under study because a high energy and high current electron beam (up to $1\mu A$ and 10 keV) are used in AES to excite Auger spectra which can produce radiation damage of oxide components. EELS permits one to decrease substantially the electron beam current and energy (up to 10 nA, 500 eV). Unfortunately, the element characteristicity in EELS is broken, so the references of all the phases are required simultaneously for concentration calculations. Some difficulties in the EELS phase analysis can be caused by presumed alteration of surface plasmon energies with the alteration of dielectric constant of the media during depth profiling of an interface, for example,

a dielectric-metal interface. The decrease of plasmon excitation probability in ultrathin layers or near interfaces can initiate some efforts to scale the phase concentrations obtained.

We employ the biplot technique using row coordinates of the \mathbf{H} and \mathbf{XH} matrices balanced by appropriate singular value multiplication to project EELS spectral intensities of the whole spectra set into the same space, where the EELS spectra are mapped [1]. If we connect the \mathbf{n} spectra points of depth profile with the origin of coordinates, it can be seen that some parts of the \mathbf{m} spectral intensity points lie near the vectors directed to clusters, trends, etc. of the spectra set. It means that such spectral intensities have significant loadings onto the corresponding spectra. The aim of this study was to define the spectral intensity intervals responsible for the occurrence of specific interfacial components in the case of sharp interphase boundaries.

3. Experimental

The depth profiling was carried out by successive cycles of ion sputtering and data accumulation on the Auger microprobe model JAMP-10S. A primary electron beam of 10 keV and 1 μA (defocused up to 100 μm to minimize radiation damage) was used for Auger and of 400 eV and 10 nA for EELS spectra excitations, respectively. The Auger spectra were measured in the derivative mode $E \times N'(E)$ with a modulation amplitude of 5 V. Accumulation time was 250 ms/eV with the energy step of 1 eV. To avoid the charging of Al_2O_3 wafers, the normal beam incidence was changed to 45° incidence by rotating the sample plane and the beam energy was lowered to 5 keV. The EELS spectra were measured in the integral mode $E \times N(E)$. The accumulation time was 500 ms/eV with the energy step of 0.5 eV. The energy resolution was about 0.01. 1 keV or 3 keV Ar^+ ion bombardment was used in accordance with the film thickness. As a rule, the sets of 50 spectra with 80 intensity points in a spectrum were representative. To exclude constant background components, the spectra were centered [1].

The Auger and EELS spectra sets of the $Al/Al_2O_3/Si$ and $YBa_2Cu_3O_{7-x}/CeO_2/Al_2O_3$ thin film oxide systems obtained in the course of ion sputtering were investigated using applied statistics methods. The characteristic features of the systems under study are both simple structure of losses and well-defined energy difference between principal loss peaks of contacting materials. To minimize the interaction of film layers coming in contact, the appropriate regimes of film production and heat treatment were used. The measured energy positions of peaks were in error by 0.5 eV.

4. Results and discussion

4.1. The Al/Al_2O_3 interface. Some of Auger spectra of the Al/Al_2O_3 system (the O KLL Auger line) are presented in Fig.1. The dimensionality of the data

space was two. With the rise of sputter time the projections of spectra into the space of the two first principal components are arranged (Fig.2) in the origin of coordinates (zero level of O KLL intensity), then on the line directed to the origin of coordinates (the uniphase region of some oxygen-containing phase in the presence of unanalyzable phase of *Al*) and after that they turn out to the point cluster corresponding to Al_2O_3 film. The composition profiles of oxygen-containing phases obtained by oblique rotation of coordinates are presented in Fig.3. The first phase corresponds to the initial state of Al_2O_3 , the other corresponds to the same Al_2O_3 phase destroyed by electron and ion beams. It should be noted that the mixture of phases at the interface in this case is not the mixture of real phases of a constant composition due to the ability of AES to sense a nearneighbourhood of exited atom.

The EELS spectra of the *Al* film, the *Al/Al₂O₃* interface and the Al_2O_3 film are presented in Fig.4. The energies of bulk *Al* plasmons (the first and the second bulk plasmons are seen at the energies of $\Delta E = 14.5eV$ and $\Delta E = 30eV$, the surface plasmons are not significant under these experimental conditions and are seen as high energy peak shoulders) correspond to the literature data. The EELS spectra of Al_2O_3 contain one wide peak corresponding to interband transitions. The dimensionality of the data space set by the EELS spectra of depth profile including the interface was three. It presumes the existence of an appreciable specific interfacial component. The biplot technique shows in the plane of the first and the second principal axes (Fig.5) that the tendency of point displacement along the line with sputter time increasing is attributed to a permanent change of contributions of spectral features with the energies of $\Delta E = 14.5eV$ (and also $30 eV$) and $\Delta E = 21eV$ in the transition region between *Al* and Al_2O_3 . This fact does not contain any new information. However, it is seen in the plane of the first and the third principal axes (Fig.6) that the rise of interfacial component content (maximum contents is observed at the sputter time of 11 min.) is attributed to spectral features with the energies of $\Delta E = 6.5eV$ and $\Delta E = 18eV$ occurred simultaneously at the interface. These features are not seen in Fig.4, but can be seen in the difference spectrum (Fig.7), that is the difference between the 11 min. spectrum and the linear combination of the *Al* and Al_2O_3 spectra composed with appropriate weights. The contribution of these features into the interface spectrum is about 0.05 of spectrum intensity. The energies of the features obtained by the biplot technique are exactly equal to the difference and half-sum of the energies of principal spectral features of *Al* (bulk plasmon) and Al_2O_3 (interband transitions) films coming in contact. As can be seen further this phenomenon is registered on a great variety of interfaces which corresponds to both simple structure of losses and well-defined energy difference of principal loss peaks of contacting materials. We can furnish an explanation of it as the interaction of collective excitations (and interband transitions in a particular case) at the analyzed interface under electron beam, that is the adventition of the beats in a system of harmonic oscillators (for example, oscillations which take place

with some frequency corresponding to the energy of $\Delta E = 14.5eV$) under an external periodic force ($\Delta E = 21eV$). Earlier the occurrence of a peak with the energy of $\Delta E = 7.1eV$ in the EELS spectra of ultrathin Al_2O_3 films obtained by in situ oxidation of Al was observed [6]. Phenomenological dielectric theory was used in [7] to interpret this peak as a modified Al surface plasmon peak shifted on an energy scale due to the alteration of dielectric constant of the media. The proposal about the existence of a surface plasmon excitation with the energy of $\Delta E_s = ((\Delta E^2 + \Delta E'^2)/2)^{1/2}$, where ΔE and $\Delta E'$ are the bulk plasmon energies of contacting materials (metals), was also suggested in [7]. Despite of the fact that this value is close to the value of a half-sum of the energies of the principal loss peaks obtained, we believe that there is another physical phenomenon. Both the constancy of "modified" plasmon energy at the interface region with varied phase composition and the simultaneous occurrence of two types of energy losses corroborate our conclusion.

1.2. To minimize the electron and ion beam radiation effects on the interface EELS spectra registration, the model system Sn/Si was studied. The Sn film was obtained at liquid nitrogen temperature by rf magnetron deposition on the Si wafer cleaned in rf plasma to remove a native oxide. There was no Sn continuous coating, but we believe that the interface is sharp and the diffusion interaction of Sn and Si is negligible. The EELS spectra of the Sn film and the Si wafer with their interface obtained in the course of depth profiling are presented in Fig.8. The system under study was more complex than the previous one due to a high dimensionality of the data space (attributed to the surface plasmon intensity alteration) but it is seen (Fig.9) that the specific spectral feature with the energy of $\Delta E = 14.5eV$ equal to the half-sum of the energies of the principal loss peaks ($\Delta E = 12.5eV$ and $\Delta E = 16.5eV$) of Sn and Si also exists. The feature with a difference energy comes into elastic peak region.

1.3. The Bi/Si system was investigated to confirm the results obtained earlier. The absence of any new phase at film-substrate interface was confirmed by Auger depth profiling. The EELS spectra of the Bi film, the Si substrate and their interface are presented in Fig.10. The specific interface features are seen in Fig.11: with the energy of $\Delta E = 7eV$ corresponding to the difference of $\Delta E = 16.5eV(Si)$ and $\Delta E = 9.5eV(Bi)$, with the energy of $\Delta E = 19eV$ corresponding to the difference of $\Delta E = 33eV(Si)$ and $\Delta E = 14eV(Bi)$, with the energy of $\Delta E = 23eV$ corresponding to the difference of $\Delta E = 33eV(Si)$ and $\Delta E = 9.5eV(Bi)$ and, also, to half-sum of $\Delta E = 33eV(Si)$ and $\Delta E = 14eV(Bi)$. The dimensionality of the data space was three that points to the existence of unique interfacial component with 7, 19 and 23 eV features.

2. The $YBa_2Cu_3O_{7-x}/CeO_2/Al_2O_3$ system.

2.1. The $YBa_2Cu_3O_{7-x}/CeO_2$ interface. Some content of a new phase (up to 0.3, connected with thermal decomposition of $YBa_2Cu_3O_{7-x}$) was detected at the interface by Auger depth profiling (Fig.12). The identity of phase composition profiles obtained by the Cu LMM and Ba MNN Auger line studies supports the assumption that the existence of a new phase mixture is also pos-

sible. Electron and ion beams in the AES mode modifies the CeO_2 film not only at the interface but also in the CeO_2 film bulk as can be seen from the Ce MNN Auger line study (the CeO_2 concentrations were plotted on the base of p-to-p Ce MNN intensities for the sputter times higher than 15 min.). It should be mentioned that the existence of a real new phase at the $YBa_2Cu_3O_{7-x}/CeO_2$ interface is not an authentic fact due to the absence of the data for higher temperature depositions of the $YBa_2Cu_3O_{7-x}$ film and small thickness of the interfacial layer as compared with the depth resolution. There is a mismatch of phase concentrations of CeO_2 obtained by the analysis of the Ce MNN Auger inelastic losses in the Ba MNN Auger line region and the CeO_2 concentrations obtained by the analysis of the Ce MNN Auger line. Therefore, the study of electron energy losses is important in AES.

Despite of possible existence of a new phase at the interface, the EELS spectra study was performed. The EELS spectra of the $YBa_2Cu_3O_{7-x}$ film (principal features are with the energies of $\Delta E = 12.5eV$ and $\Delta E = 23eV$), the CeO_2 film (principal features are with the energies of $\Delta E = 13eV$ and $\Delta E = 28.5eV$) and their interface are presented in Fig.13. The specific interfacial features of low intensities with the energies equal to the difference and half-sum of the energies of principal loss peaks with the energies of $\Delta E = 12.5eV$ and $\Delta E = 28.5eV$ are designated in Fig.14 by arrows.

2.2. The CeO_2/Al_2O_3 interface. There are (Fig.15-16) specific interfacial features of low intensities with the energies of $\Delta E = 8eV$ and $16.5 eV$ equal to the difference and half-sum of the energies of principal loss peaks with the energies of $\Delta E = 13eV(CeO_2)$ and $\Delta E = 21eV(Al_2O_3)$. The concentration profiles of Al -containing phases were identical with those presented in Fig.3.

5. Conclusions

The AES depth profiling study of thin oxide film systems indicates that there always exists an interfacial oxide layer where the modification of composition by electron and ion beams occurs. The EELS spectra are not sensitive to this process. On the other hand, the specific interfacial features corresponding to a distinct interaction of collective excitations (and interband transitions) at the interphase boundaries of contacting materials occur in the absence of a new phase formation. This fact appreciably lowers the analytic usefulness of EELS as a method of phase analysis. The interaction defined is responsible only for a few percents of spectral intensities of the analyzed interface in its maximum and is not of long-range order.

The work was supported by Russian Foundation for Basic Research, grant 97-03-33557.

References

1. Handbook of Applicable Mathematics. Volume VI: Statistics. Part B. / Eds. W. Ledermann and E. Lloyd. - N.Y.: Wiley, 1984.
2. Aivazyan S.A., Buchstaber V.M., Yenyukov I.S., Meshalkin L.D. Applied Statistics: classification and reduction of dimensionality. - Moscow: Finansy i statistika, 1989.
3. Malinowski E.R., Howery D.J. Factor Analysis in Chemistry. - N.Y.: Wiley, 1980.
4. Beshenkov V.G., Kopetskii Ch.V., Shiyonov Yu.A. Phys. Stat. Sol. (a). 1989. V. 114. P. 191.
5. Beshenkov V.G., Znamenskii A.G., Marchenko V.A. Izvestiya RAN. Ser. fiz. 1998. V. 62. No 3. P. 517.
6. Powell C.J., Swan J.B. Phys. Rev. 1960. V. 118. P. 640.
7. Stern E.A., Ferrell R.A. Phys. Rev. 1960. V. 120. P. 130.

FIGURE CAPTIONS

Fig. 1. The derivative O KLL Auger spectra of Al/Al_2O_3 . The values of sputter time (in min.) corresponding to the spectra are designated.

Fig. 2. The projections of the O KLL Auger spectra of Al/Al_2O_3 onto the plane of the first and the second principal components. The values of sputter time (in min.) corresponding to the spectra are designated.

Fig. 3. The composition profiles of oxygen-containing phases of Al/Al_2O_3 in depth: the initial Al_2O_3 phase (circles) and the Al_2O_3 phase modified by electron and ion beams (squares).

Fig. 4. The EELS spectra of Al/Al_2O_3 : the Al film (circles), the Al_2O_3 film (squares) and the Al/Al_2O_3 interface (triangles).

Fig. 5. The Al/Al_2O_3 biplot map: the EELS spectra in depth (squares), the EELS spectral intensities of the whole depth profile (circles) projected onto the plane of the first and the second principal axes ($j=1,2$). The values of sputter time (in min.) corresponding to the spectra and the energies of principal features are designated.

Fig. 6. The Al/Al_2O_3 biplot map: the EELS spectra in depth (squares), the EELS spectral intensities of the whole depth profile (circles) projected onto the plane of the first and the third principal axes ($j=1,3$). The values of sputter time (in min.) corresponding to the spectra and the energies of principal features are designated.

Fig. 7. The EELS spectrum of Al/Al_2O_3 (up triangles) and its projection onto the plane of the first and the second principal components (down triangles) and the difference spectrum (stars).

Fig. 8. The EELS spectra of Sn/Si : the Sn film (circles), the Si substrate (squares) and the Sn/Si interface (triangles).

Fig. 9. The Sn/Si biplot map: the EELS spectra in depth (squares), the EELS spectral intensities of the whole depth profile (circles) projected onto the plane of the first and the third principal axes ($j=1,3$). The values of sputter time

(in min.) corresponding to the spectra and the energies of principal features are designated.

Fig. 10. The EELS spectra of *Bi/Si*: the *Bi* film (circles), the *Si* substrate (squares) and the *Bi/Si* interface (triangles).

Fig. 11. The *Bi/Si* biplot map: the EELS spectra in depth (squares), the EELS spectral intensities of the whole depth profile (circles) projected onto the plane of the first and the third principal axes ($j=1,3$). The values of sputter time (in min.) corresponding to the spectra and the energies of principal features are designated.

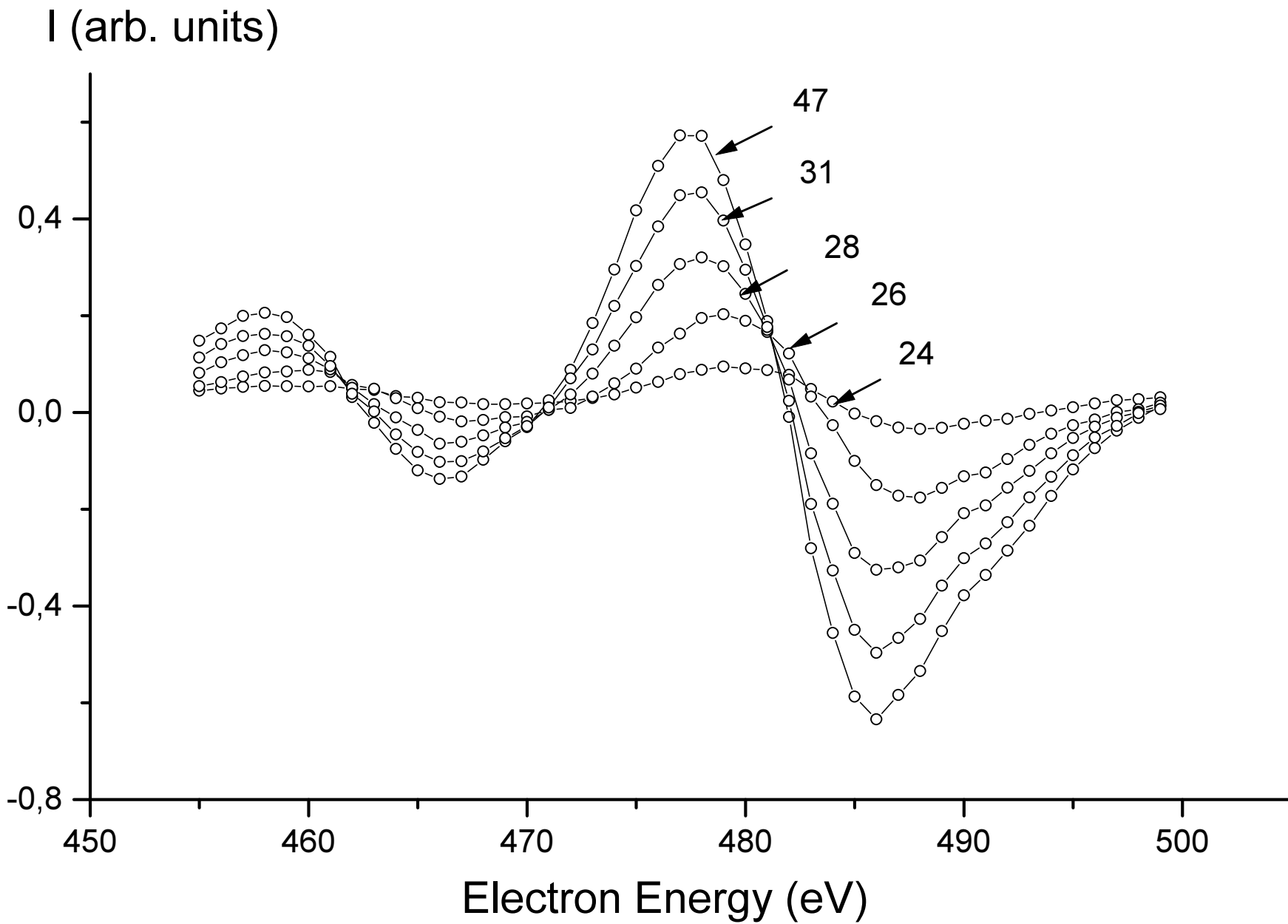
Fig. 12. The composition profiles of $YBa_2Cu_3O_{7-x}/CeO_2$ in depth: the initial $YBa_2Cu_3O_{7-x}$ phase (circles), the initial CeO_2 phase (down triangles), the CeO_2 phase modified by electron and ion beams (squares) and the new phase at the interface (up triangles).

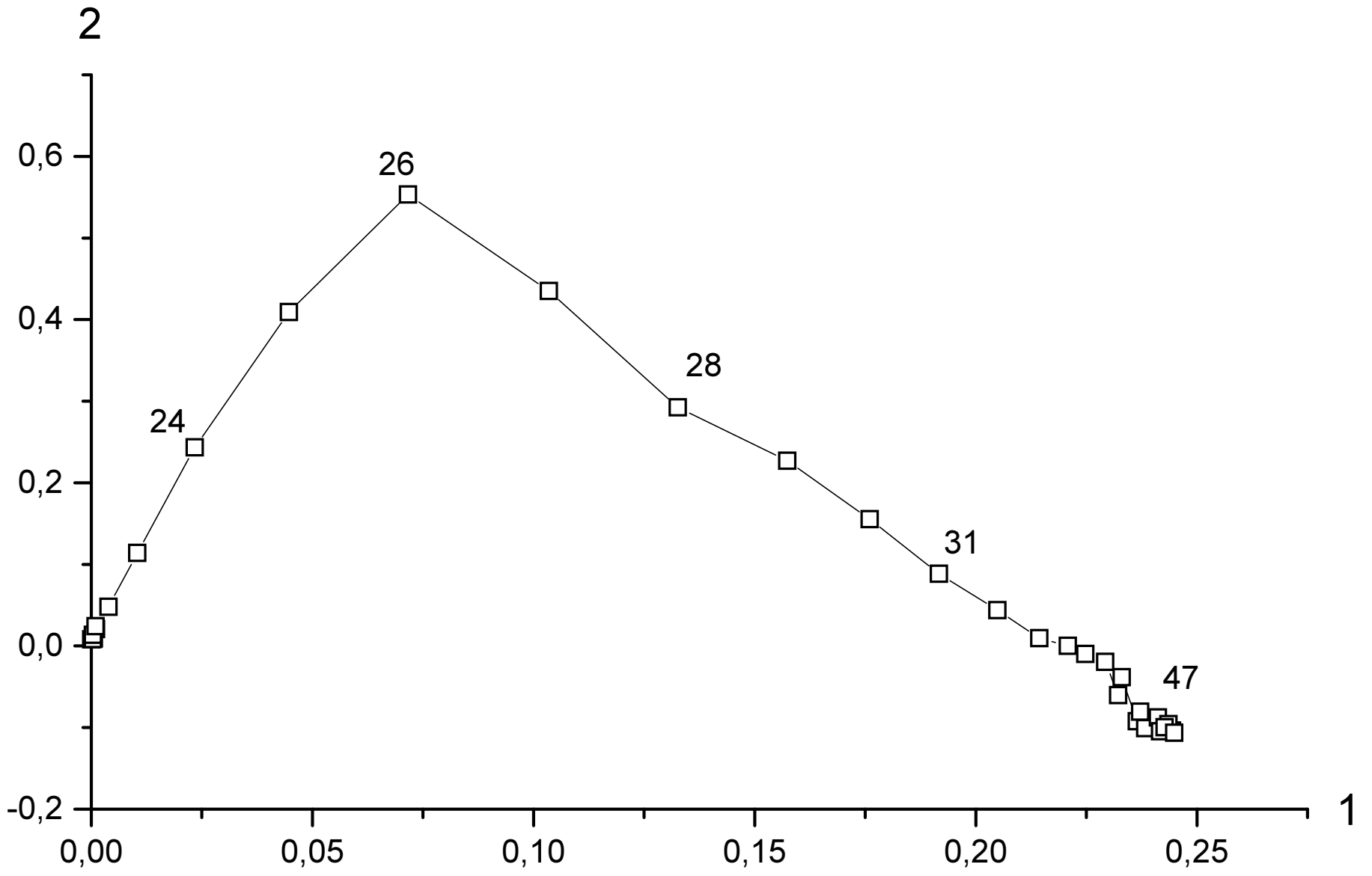
Fig. 13. The EELS spectra of $YBa_2Cu_3O_{7-x}/CeO_2$: the $YBa_2Cu_3O_{7-x}$ film (circles), the CeO_2 film (squares) and the $YBa_2Cu_3O_{7-x}/CeO_2$ interface (triangles).

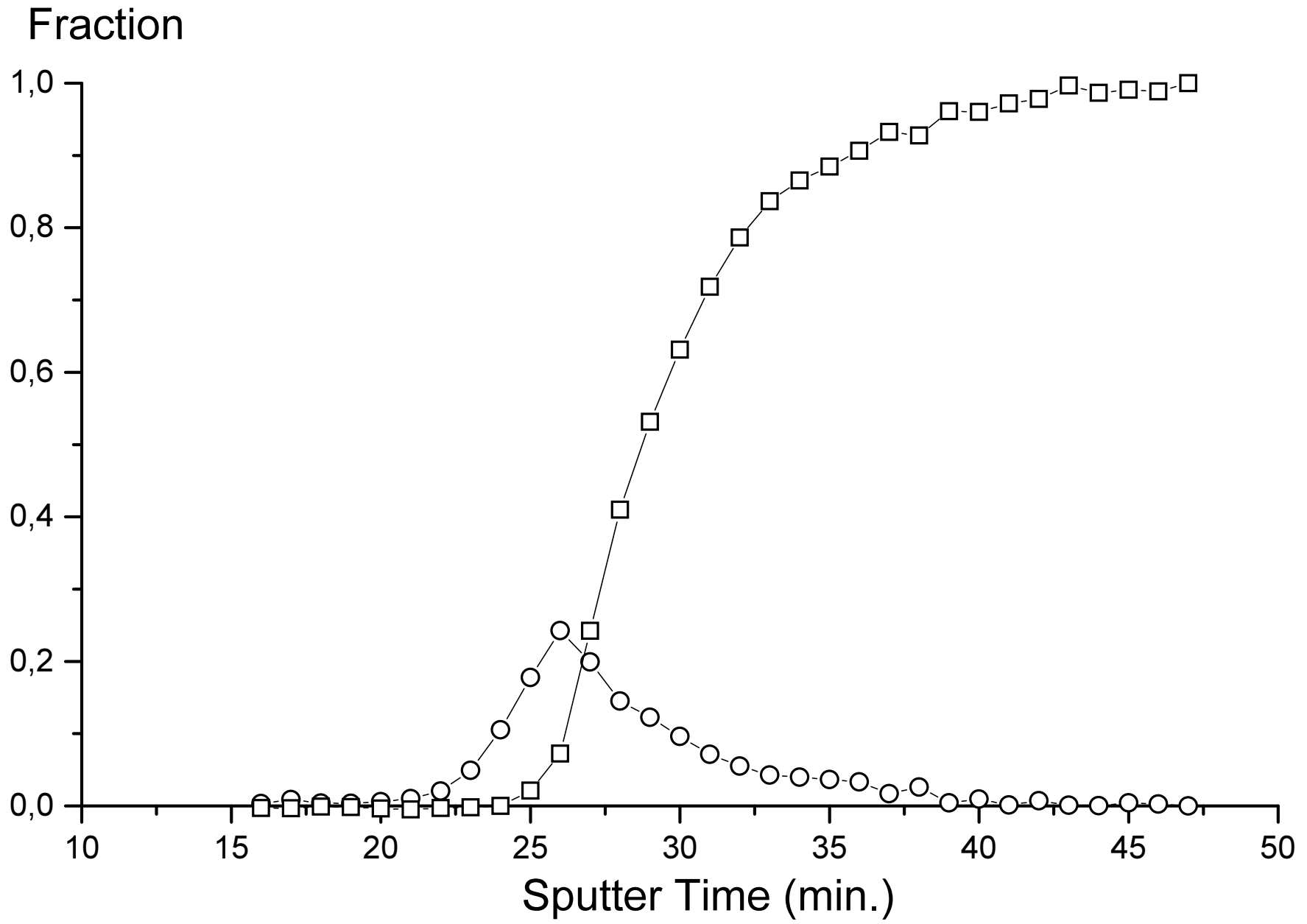
Fig. 14. The $YBa_2Cu_3O_{7-x}/CeO_2$ biplot map: the EELS spectra in depth (squares), the EELS spectral intensities of the whole depth profile (circles) projected onto the plane of the first and the third principal axes ($j=1,3$). The values of sputter time (in min.) corresponding to the spectra and the energies of principal features are designated.

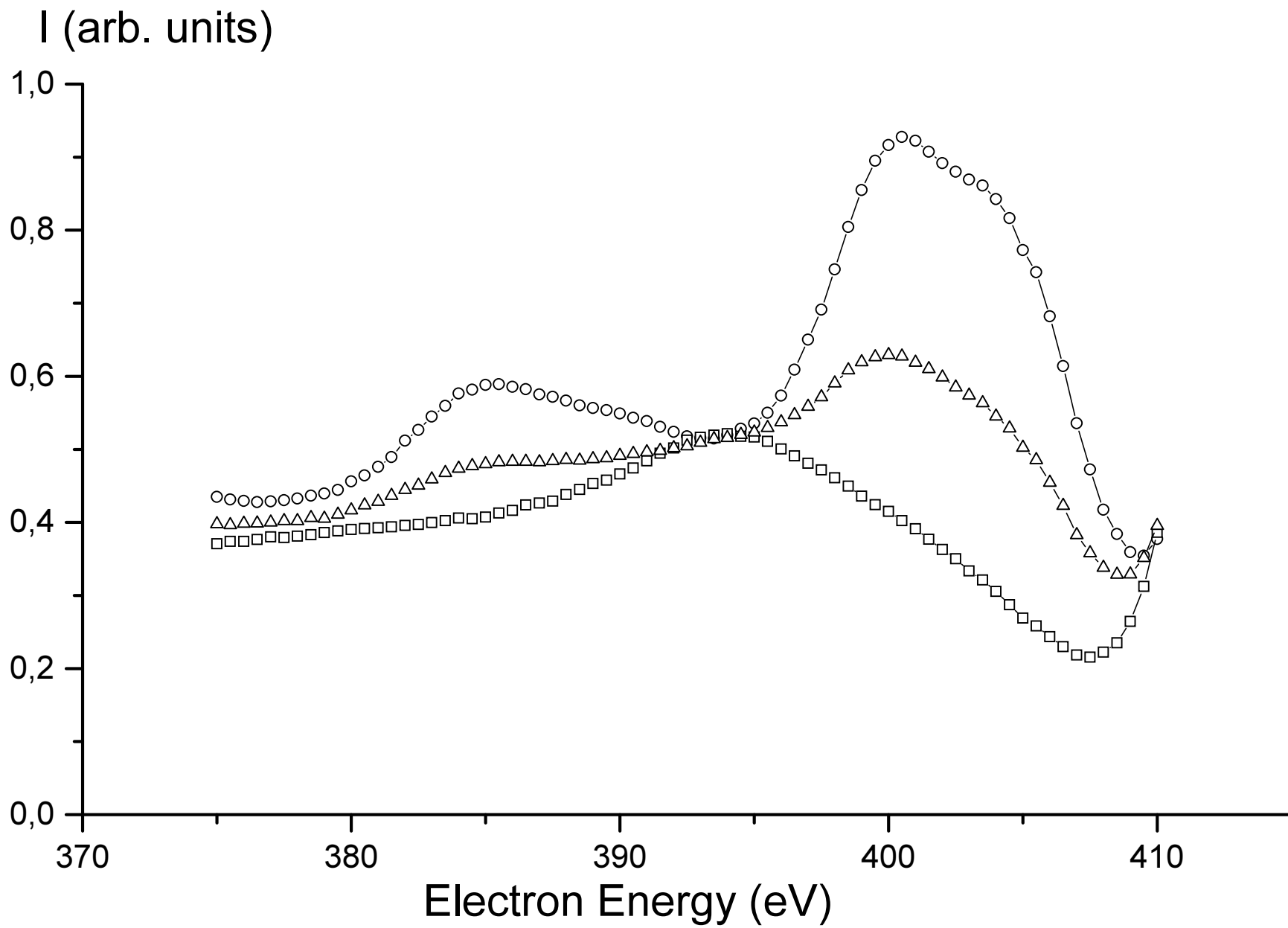
Fig. 15. The EELS spectra of CeO_2/Al_2O_3 : the CeO_2 film (circles), the Al_2O_3 substrate (squares) and the CeO_2/Al_2O_3 interface (triangles).

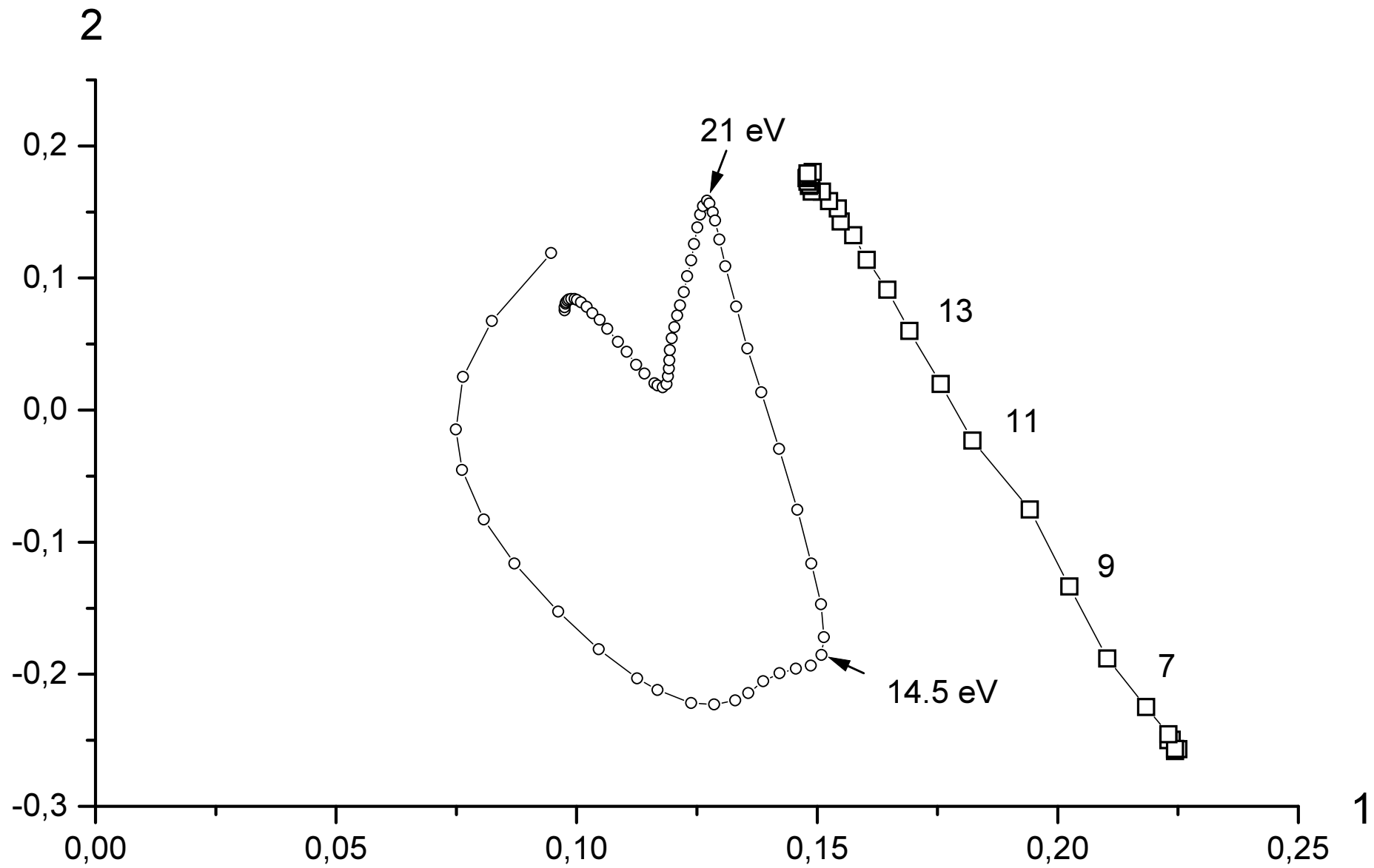
Fig. 16. The CeO_2/Al_2O_3 biplot map : the EELS spectra in depth (squares), the EELS spectral intensities of the whole depth profile (circles) projected onto the plane of the first and the third principal axes ($j=1,3$). The values of sputter time (in min.) corresponding to the spectra and the energies of principal features are designated.

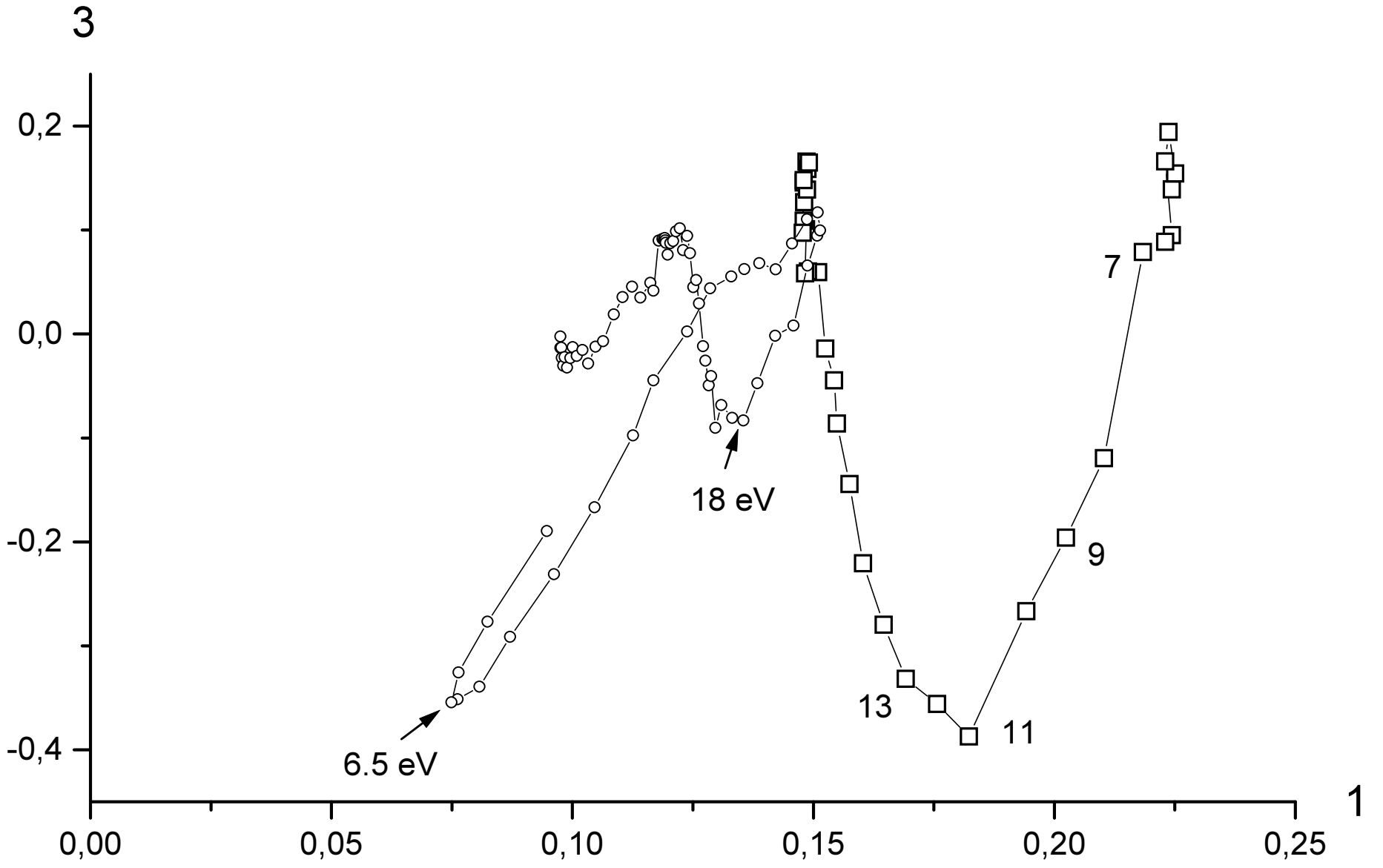


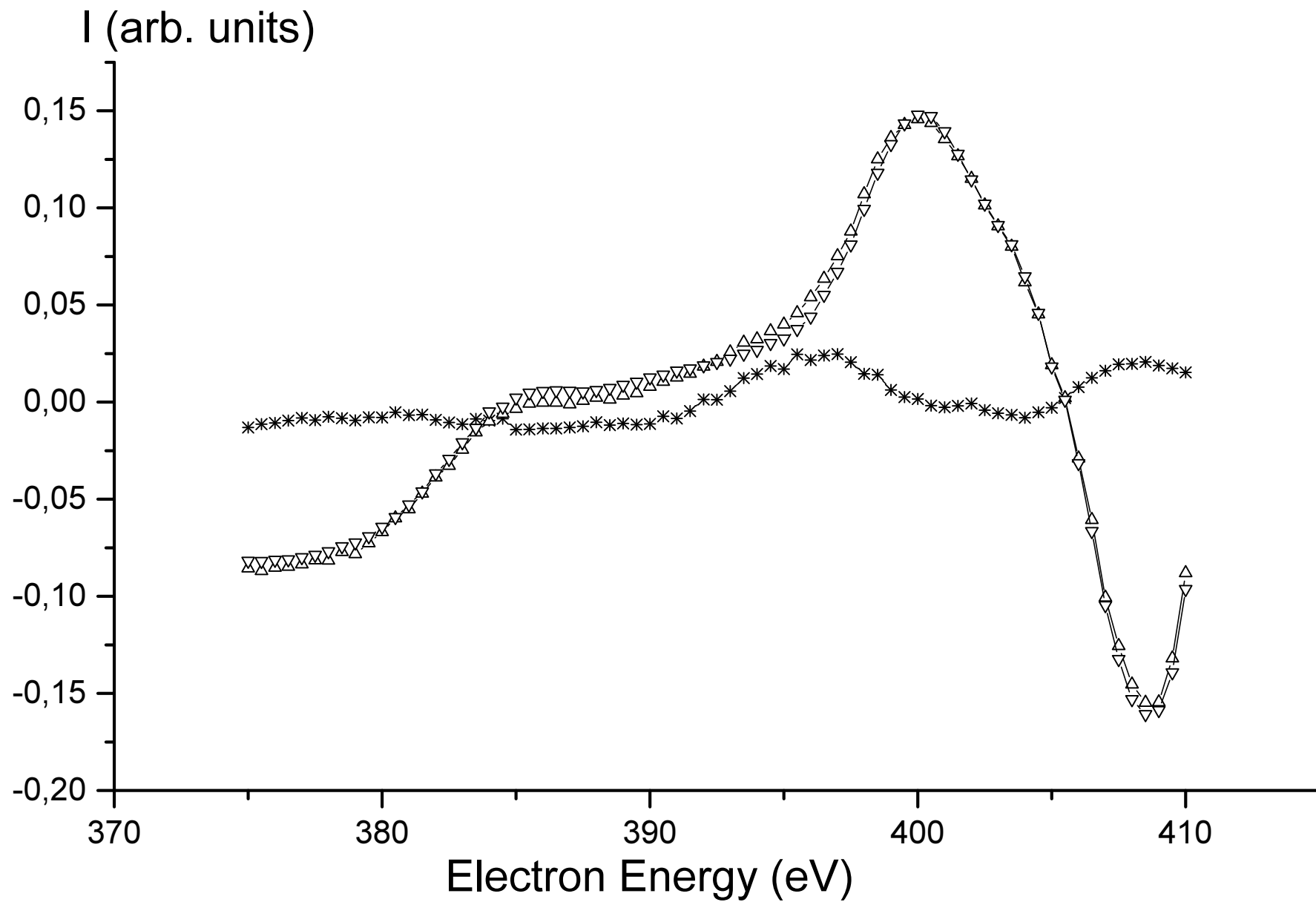


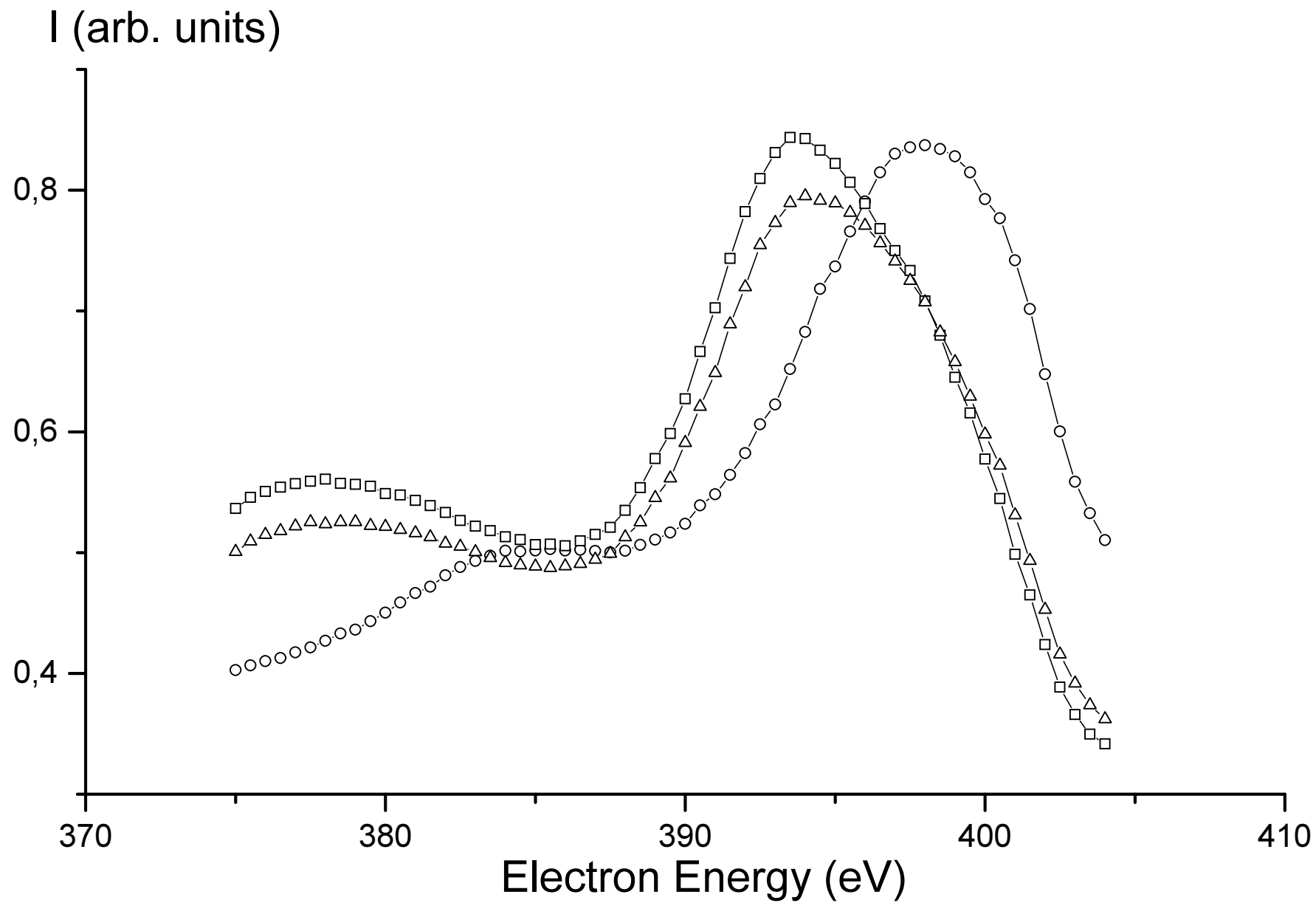


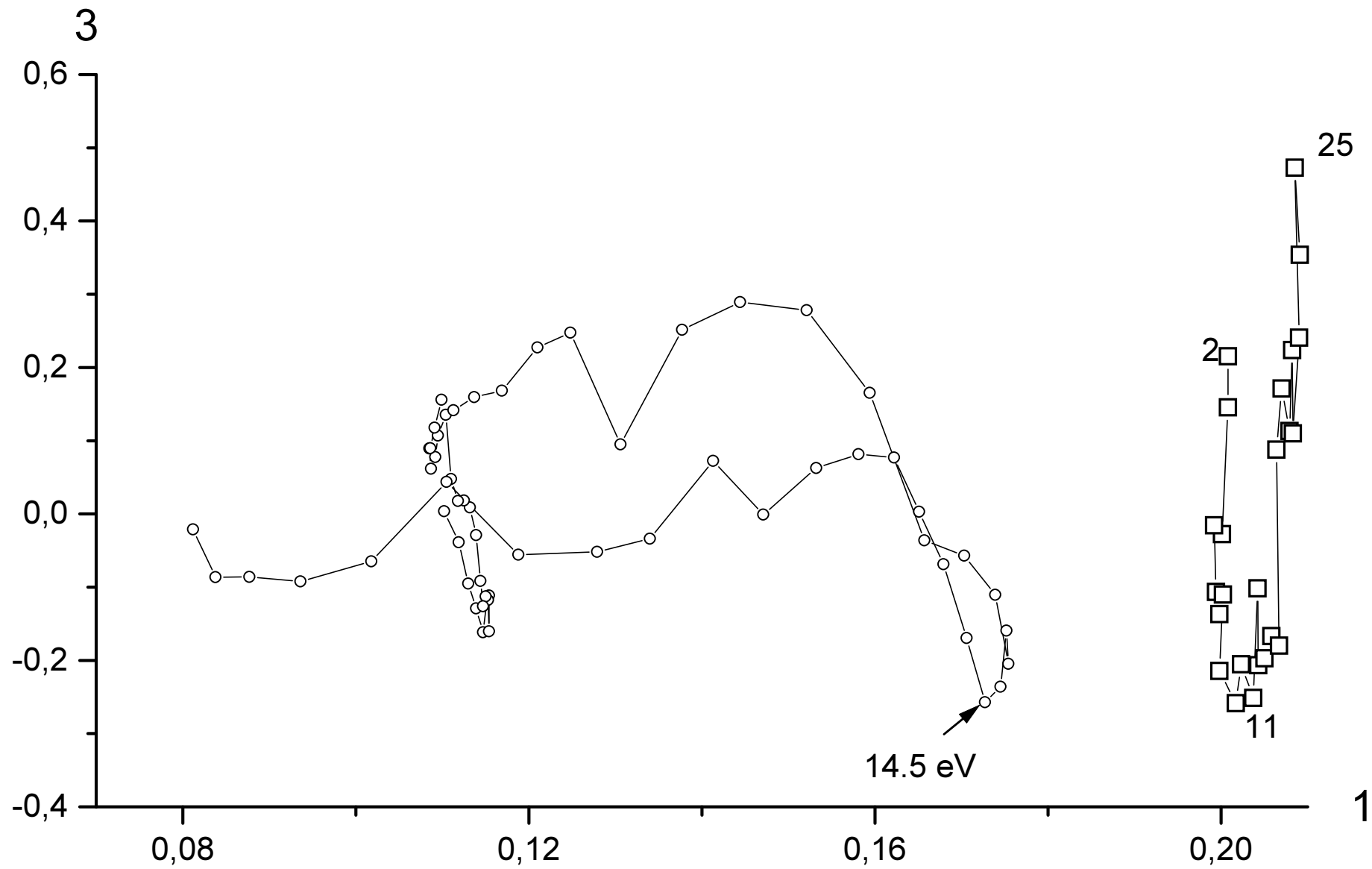


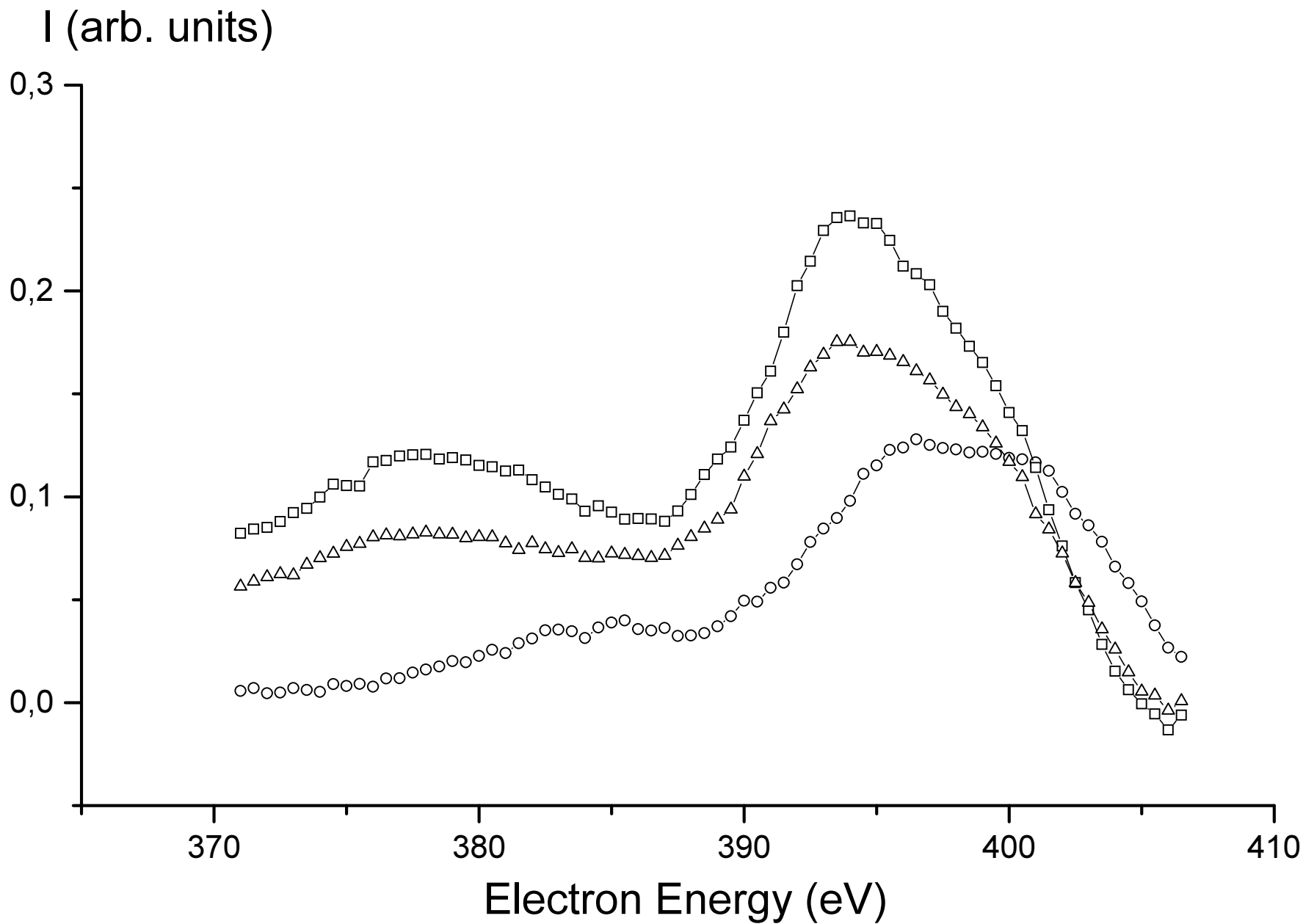


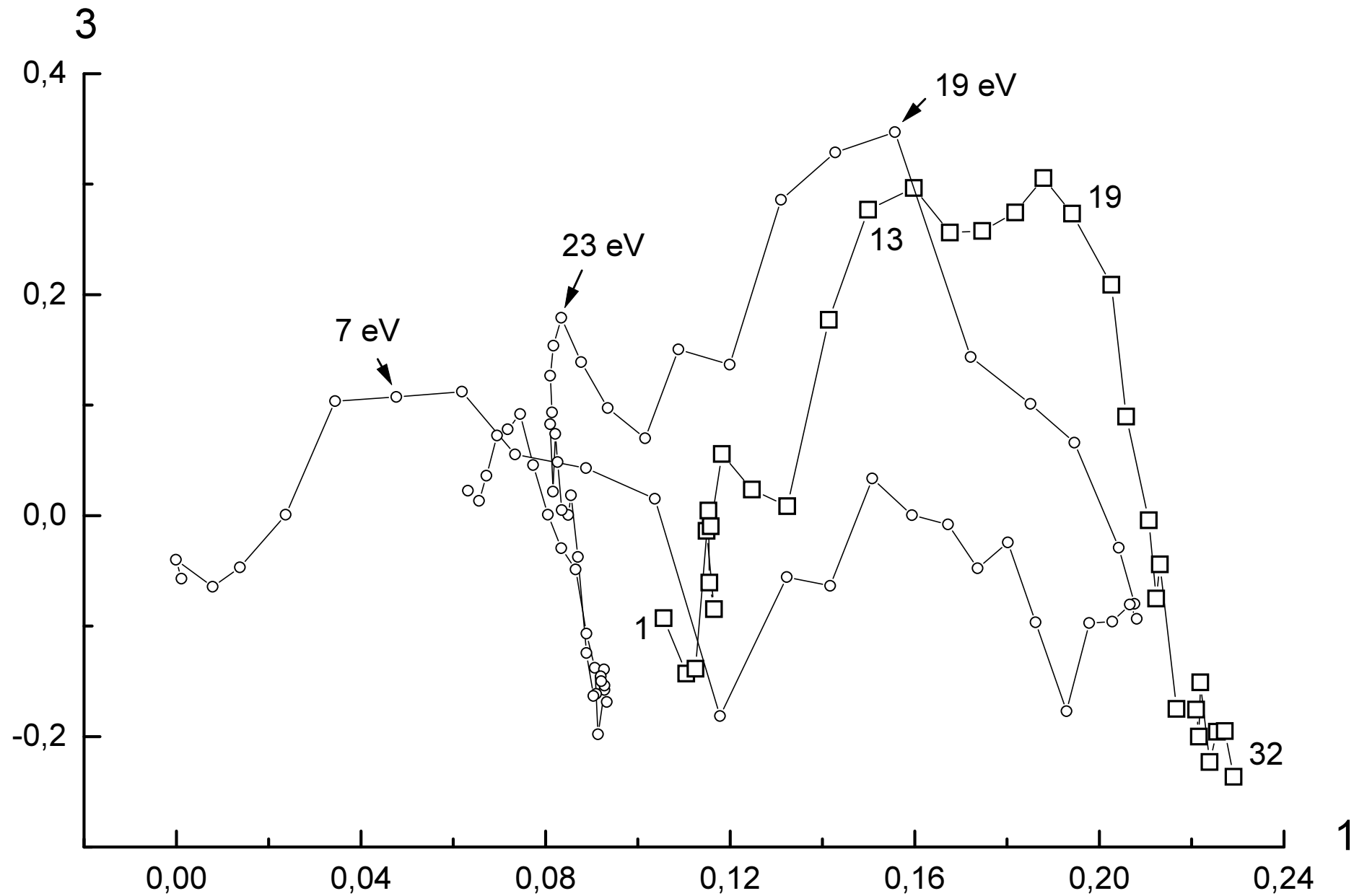












Fraction

